IEEE Photonics Journal
An IEEE Photonics Society Publication

Invited Paper

InGaAs Communication Photodiodes: From Low- to High-Power-Level Designs

Volume 2, Number 3, June 2010

M. Achouche
G. Glastre
C. Caillaud
M. Lahrichi
M. Chtioui
D. Carpentier

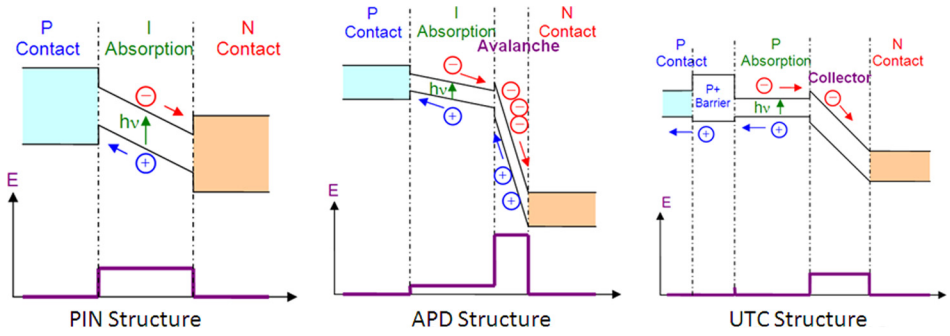

DOI: 10.1109/JPHOT.2010.2050056
1943-0655/$26.00 ©2010 IEEE

IEEE photonics SOCIETY

IEEE

InGaAs Communication Photodiodes: From Low- to High-Power-Level Designs

M. Achouche, G. Glastre, C. Caillaud, M. Lahrichi, M. Chtioui, and D. Carpentier

(Invited Paper)

Alcatel Thales III–V Lab, joint lab: Bell Labs and Thales Research Technology, 91460 Marcoussis, France

DOI: 10.1109/JPHOT.2010.2050056
1943-0655/$26.00 ©2010 IEEE

Manuscript received March 16, 2010; revised April 29, 2010; accepted May 3, 2010. Date of publication May 6, 2010; date of current version June 8, 2010. Corresponding author: M. Achouche (e-mail: mohand.achouche@3-5lab.fr).

Abstract: While InGaAs absorption material has been used for various applications up to 1.6-μm wavelength, specific designs for low-level detection have become of main interest using high responsivity and low-dark-current detectors. By adding an avalanche multiplication layer to form an avalanche photodiode (APD) using the Separated Absorption and Multiplication (SAM) structure, one can take advantage of the very low-noise properties of the multiplication process in large-bandgap Al(Ga)(In)As material to improve receiver sensitivity by $>$ 10 dB. Under high-power-level injection, specific PIN structures have been developed to improve space charge effects and linear operation as needed for power applications such as high bit rates using coherent detection or analog photonic links. Specific designs to achieve simultaneously broad bandwidth, high responsivity, very high power saturation, and high linearity will be discussed.

Index Terms: Photodiodes, InGaAs, avalanche photodiodes, APDs, SAM, microwave photonics, analog links.

1. Introduction

InGaAs/InP photodiodes have been developed for several years for telecommunication applications, owing to the near-infrared sensitivity of $In_{0.53}Ga_{0.47}As$ grown lattice-matched onto Indium Phosphide [1]. Remarkable progress has been achieved on epitaxial layers growth by Metallic Organo Vapor Phase Epitaxy (MOVPE) and molecular beam epitaxy (MBE) techniques with low residual doping and precise control of various heterostructure interfaces. Good electrical characteristics as low dark current at room temperature and high quantum efficiency have been demonstrated so far on PIN photodiodes with high-speed operation capabilities that are compatible with present optical broadband transmission systems [2]. These characteristics can even now be achieved on large-area wafers (3- and 4-in InP) with good material homogeneity.

Avalanche photodiodes (APDs) are attractive devices because they combine simultaneously detection and amplification properties in one single device, enabling an improvement of the photoreceiver sensitivity by more than 10 dB compared with PIN photodiodes. APD performances are related to electron and hole ionization coefficients (respectively, α and β) in the multiplication region; better performance is achieved when the ratio $k = \alpha/\beta$ deviates markedly from unity [3]. Indium Phosphide, with a k value of 2, has traditionally been used in APDs for 1.55-μm applications. The structure used is called Separate Absorption and Multiplication (SAM) because the absorption

and multiplication regions are separated. Such APDs are well suited for low-dark-current applications, but their moderate gain–bandwidth product (< 80 GHz) restricts the frequency response of the detector at high avalanche gains [4]. Recently, very low-noise APDs were demonstrated using a wide range of very thin avalanche layers, including InP, $Al_xIn_{1-x}As$, GaAs, $Al_xGa_{1-x}As$, etc. For example, some compositions of $Al_xGa_{1-x}As$ $(x \geq 0.8)$ appear to exhibit very low excess noise corresponding to an effective impact ionization coefficients ratio 1/k $\sim$ 0.15 to 0.19 [5]. These results suggest that very thin $Al_{0.8}Ga_{0.2}As$ avalanche widths can be used to achieve APDs with very high speed and very low noise. Similar low-noise properties have been demonstrated with $Al_{0.48}In_{0.52}As$ avalanche material which, in contrast to $Al_{0.8}Ga_{0.2}As$, can be grown lattice-matched to InP for digital telecommunication applications and for which an ionization ratio 1/k $\sim$ 0.15 to 0.25 has been demonstrated [6].

In contrast, moving to 100-Gb/s WDM transmission using quadrature phase-shift keying (QPSK) format with a coherent receiver or for analog multichannel links, the photodetector should withstand high optical power with high linearity. Traditional PIN photodiodes show early saturation due to large densities of carriers generated in the depletion region which disturb the electric-field distribution and hence reduce carrier drift velocity. This so-called "space charge effect" limits large-signal saturation current to 10–20 mA at 20 GHz [7]. To overcome this limitation, several new designs have been proposed including: partially depleted absorber (PDA) photodiode that uses a thin depleted absorption layer followed by a p-doped absorption layer [8] and uni-travelling-carrier (UTC called also unipolar) photodiodes. Unipolar photodiodes are most likely the powerful structure to reduce space charge effect limitations since they use only electrons as active carriers [9]. Recently, UTCs demonstrated very high saturation powers in the range of 50–100 mA at 20 GHz orienting photodiode designs toward power dissipation effectiveness and thermal effect reduction [10]. Using a waveguide UTC structure allows us to even increase the responsivity at a higher bit rate.

This paper reviews recent developments of InGaAs APD designs, which allow high-sensitivity photoreceivers operating in the 1.55-μm wavelength window to become the enabling architecture for next-generation metro/access applications at bit rates > 10 Gb/s. New vertical InGaAs power photodiode designs and waveguide UTC structures will also be discussed. Several UTC photodiode structures will be presented, with emphasis on saturation performances at 20 GHz. The monolithic integration of a lensed mirror facet to increase coupling efficiency or saturation mechanisms will be underlined.

2. InGaAs APDs Designs

APDs are very attractive photodetectors for many applications (telecom, ranging, sensing, spectroscopy, ...) because they provide internal gain arising from avalanche multiplication of carriers photogenerated during the absorption of light. There are two factors that limit the APD performances:

a. gain uncertainty (or multiplication noise) characterized by the excess noise factor f(M);
b. avalanche build-up time, which is the time needed for all carrier multiplication events to complete (gain–bandwidth product is a practical APD characteristic linked to build-up time). According to local-field avalanche theory [3], both multiplication noise and gain–bandwidth product of APDs are determined by $k = \alpha/\beta$.

Since the ionization ratio represents a material property, for a given electric field, efforts to improve APD performance have traditionally focused on new materials investigation and electric-field optimization. Two III–V materials of interest have emerged: AlGaAs and AlInAs, lattice-matched to GaAs and InP, respectively, both characterized by a wide bandgap [5], [6]. Today, AlInAs is incorporated into the multiplication region of SAM APDs by several groups. For example, a front-side illuminated AlInAs APD has been realized by Mitsubishi for 10-Gb/s systems using MBE material and has demonstrated a low dark current of 160 nA at $0.9 \times V_{br}$ (V_{br} is the breakdown voltage) and a gain–bandwidth product of 120 GHz [11].

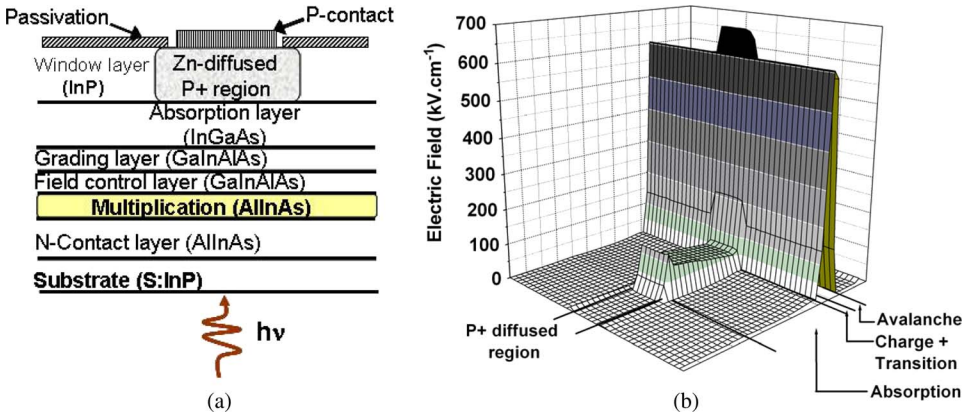

Fig. 1. (a) Schematic cross section of backside-illuminated AlInAs APD and (b) calculated electric-field distribution.

Robust APDs are based on planar junction technology using Zn-diffusion process, as shown in Fig. 1(a), for a typical backside-illuminated AlInAs APD. As a consequence, a natural guard ring is formed for this electron-injection-initiated avalanche process, as shown in Fig. 1(b), where simulation results using drift-diffusion model of electric-field distribution along the APD is shown. Indeed, electric fields at the edge of the mesa-diode are lower than under the central P-N junction, allowing improved surface stability compared with mesa-type diode.

The typical epitaxial structure of the SAM APD shown in Fig. 1(a) is grown by MOVPE on an n-doped InP substrate. The vertical structure includes from the top an unintentionally doped InP window layer (1 μm) followed by an unintentionally doped InGaAs absorption layer (1.2 μm) and an unintentionally doped AlInAs avalanche layer (0.2 μm). An InGaAlAs grading layer (0.1 μm) is inserted between absorption and avalanche layers to avoid carriers trapping during transport between both layers. In addition, a highly p-doped AlInAs charge layer is used to confine high avalanche electric field in the multiplication layer. Precise control of this shield charge doping is required in order to prevent dopant spreading during Zinc diffusion process used for the fabrication of the planar junction and which occurs at a high temperature ($> 500\ ^{\circ}\mathrm{C}$). Two dopant impurities are possible for charge layer using MOVPE technique: Zinc and Carbon. Charge dopant spreading during processing results in lower effective charge doping that increases electric field in the absorption region.

Fig. 2(a) shows a typical dark current versus reverse bias for various measurement temperatures of a Carbon-doped AlInAs APD (30-μm-diameter diode). Clear and clean *I–V* characteristics are measured whatever the temperature attesting of smooth transition from absorption to avalanche layers thanks to the well-controlled AlGaInAs grading layer. Indeed, due to the potential step in the conduction band between InGaAs and AlInAs, the photogenerated carriers in the InGaAs absorption region are separated by the electric field, and the corresponding electrons jump into the AlInAs multiplication layer by thermal energy. At low temperature, the electric field and the thermal energy are small enough that most of the carriers recombine before jumping across the step, inducing a reduction of the diode responsivity. To increase the transition rate of the electrons, an AlGaInAs grading layer is placed between InGaAs and AlInAs to grade the conduction band discontinuity.

For much low-level light detection (ranging, sensing, cryptography, ...), multiplied dark current I_{dM} is a critical parameter that needs to be reduced to improve the signal-to-noise ratio at high multiplication gain ($I_{dark} = M \times I_{dM} + I_{d0}$, where I_{d0} is the unmultiplied dark current) [12]. I_{dM} was identified as a volume contribution originating from photogenerated carriers in the absorption layer that are injected in the avalanche layer by the central region of the junction where the avalanche electric field is maximum. Fig. 2(b) compares $I_{dark} - M$ characteristics of two APDs (30-μm diameter) fabricated using, respectively, Zinc and Carbon as a dopant impurity of the charge layer.

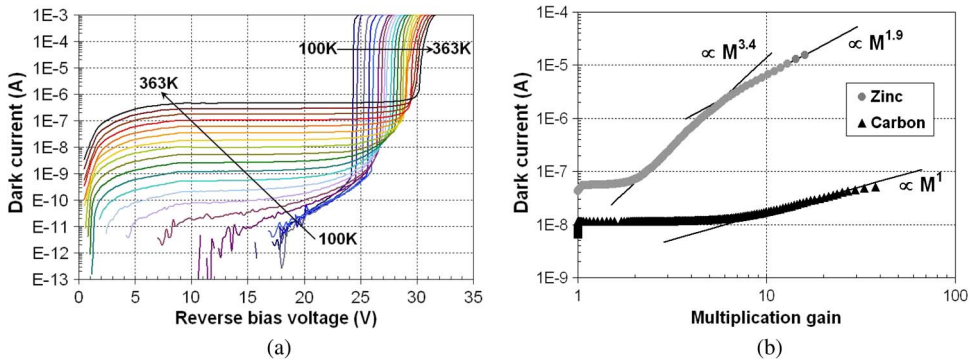

Fig. 2. (a) Typical *I–V–T* characteristics of C-AlInAs APD and (b) comparison of I_{dark} versus M of Zn- and C-APDs.

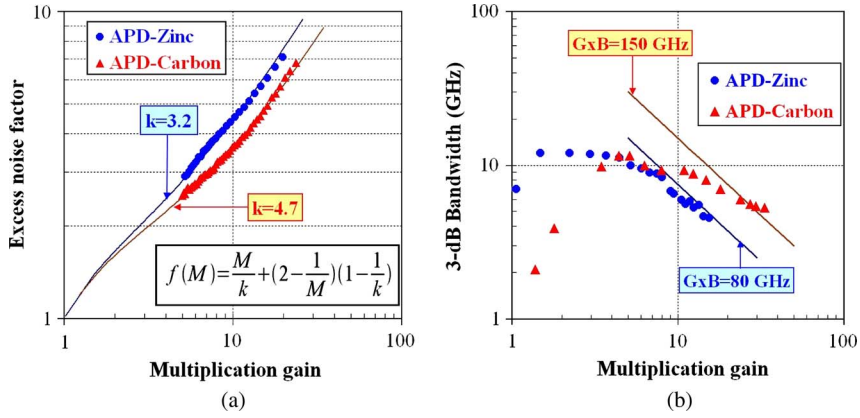

Fig. 3. Comparison of (a) excess noise factor and (b) gain-bandwidth product of C- and Zn-AlInAs APD, respectively.

While Carbon-APD demonstrates linear dark current behavior versus multiplication gain, Zinc-APD shows additional contributions to multiplied dark current I_{dM}, probably originating from unwanted multiplication in absorption layer due to Zinc-spreading. Typical multiplied dark current for fiber optics Carbon-doped APDs operating at 10 Gb/s is 1–2 nA.

In addition to impact multiplied dark current, electric-field distribution can degrade the excess noise of the avalanche diode. Very low-noise properties are achieved using AlInAs APDs when accurate charge shield doping is ensured. Indeed, comparing noise behaviors of C- and Zn-AlInAs APDs clearly shows this phenomenon, as displayed in Fig. 3(a). A very low excess noise factor $f(M = 10) = 3.5$ is deduced for C-AlInAs APD, while $f(M = 10) = 4.5$ for Zn-APD. According to the McIntyre model [3], the corresponding impact ionization ratios are, respectively, $k = 4.7$ for C-APD and $k = 3.2$ for Zn-APD. These avalanche material properties show the large potential of AlInAs if the electric-field distribution is accurately controlled. An improvement of the selectivity of the ionization process achieved under large k values also allows an increase of the gain–bandwidth product. A Gain $*$ bandwidth of 150 GHz has been demonstrated [12] when using C-AlInAs charge layer [see Fig. 3(b)], allowing for a given bandwidth larger practical available multiplication factors.

Based on APD receiver sensitivity criteria, one can assess the critical photodiodes characteristics used to improve overall fiber optic link performances. The sensitivity for a Bit Error Rate of 10^{-9} is

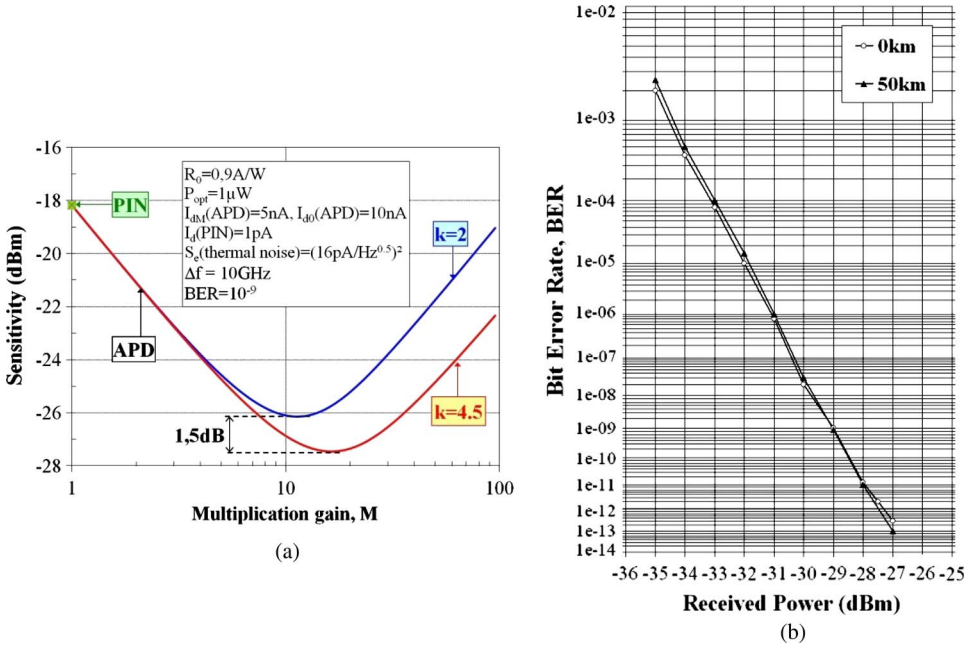

Fig. 4. (a) Calculated APD receiver sensitivity versus multiplication gain for two avalanche materials with an ionization coefficient ratio of 2 and 4.5, respectively. (b) Measured receiver sensitivity of C-AlInAs APD-TIA at 10.709 Gb/s in back-to-back and after 50-km transmission.

given by

$$(P_{\text{opt}})_{\text{min}} = \frac{qf(M)}{R_0}\left(\frac{S}{N}\right)\Delta f\left[1+\sqrt{1+\frac{2I_{\text{dM}}f(M)+\dfrac{2I_{\text{d0}}}{M^2}+\dfrac{S_e}{qM^2}}{qf(M)^2\left(\dfrac{S}{N}\right)\Delta f}}\right]$$

where f(M) is the excess noise factor, (S/N) is the signal-to-noise ratio, R_0 is the primary responsivity, Δf is the system bandwidth, I_{dM} and I_{d0} are, respectively, the multiplied and unmultiplied dark currents, and S_e is the thermal noise. Fig. 4(a) shows calculated receiver sensitivity versus multiplication factor M for two APDs with an ionization coefficient ratio k of 2 and 4.5, respectively. First, we observe 8- to 10-dB receiver sensitivity improvement using APD detectors compared with PIN photodiodes. For $M < 8$, one can see no significant difference of receiver sensitivity when increasing the ionization coefficient ratio k because the signal-to-noise ratio is only limited by the thermal noise. The impact of increasing the avalanche ionization coefficient ratio is clearly seen for larger M $(M > 10)$ because the shot noise becomes dominant, compared with the thermal noise.

Fig. 4(b) displays the bit error rate at 10.709 Gb/s of a TO-Can APD-TIA module. A sensitivity of -29 dBm is deduced with no penalty after 50-km transmission on single-mode fiber.

3. InGaAs UTC Photodiodes Designs

While for low-level light detection, photodiodes need high responsivity, low noise, and often large bandwidths, detection of high power at microwave frequencies sets challenges on bandwidth/saturation limitation, thermal dissipation, and linearity. Today, the most popular candidate for power applications is the UTC-type photodiode. By carefully separating the absorption and drift regions,

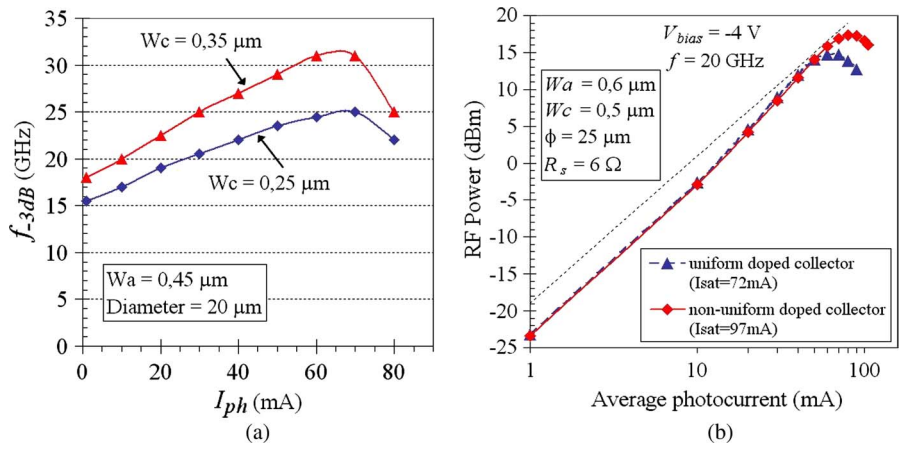

Fig. 5. (a) Large-signal 3-dB bandwidth versus photocurrent for two collector thicknesses and Vbias $= -3$ V and (b) comparison of saturation photocurrent at 20 GHz and Vbias $= -4$ V.

one can design a vertical photodiode structure with broad bandwidth and high saturation because in this situation, electrons are the unique active carriers [9].

The absorption layer of the UTC diode is p-doped, and its thickness and doping profile influence detector responsivity and transit time. The step-graded-doping profile of the p-InGaAs absorption layer allows improved transit time at low optical input power owing to a self-induced field which improves electron velocity, compared with a pure diffusion process [13]. However, for the collector design, one can find an additional degree of freedom since RC cutoff is the main parameter to take into account as collector transit time is negligible for large absorption layer thicknesses. Fig. 5(a) shows a comparison of large-signal (modulation index m $\sim$70%) 3-dB bandwidth versus the average photocurrent of two UTC photodiodes having a similar absorption layer thickness of Wa $= 0.45$ μm and, respectively, two collector layer thicknesses Wc $= 0.25$ μm and Wc $= 0.35$ μm. From this figure, a bandwidth improvement is observed at large photocurrent, which can be linked to the following:

a. reduction of junction capacitance by subtraction of the differential dynamic capacitance due to collector transit time reduction at velocity overshoot;
b. self-induced electric field in the absorption layer due to majority hole current that accelerates the minority photogenerated electrons in the absorption layer.

Worth noting is the bandwidth improvement when increasing the collector layer thickness due to a lower junction capacitance (the transit time in this layer is negligible compared with electron diffusion in absorption layer).

In Fig. 5(b), large-signal saturation current measurements at 20 GHz of two UTC detectors with two different collector designs are shown for comparison. As reported in [15], an InP nonuniformly doped collector (Wc $= 0.5$ μm) comprising a first layer composed of 0.25-μm InP n^- doped (4.10^{16} cm^{-3}) followed by a 0.25-μm InP undoped ($\sim 10^{15}$ cm^{-3}) allows a reinforcing electric field at the collector input at a large optical power input and leads to a better saturation current compared with a uniformly doped collector. The photodiode 1-dB saturation current is improved from 72 mA to 97 mA using this adapted collector design.

Saturation mechanisms observed at high optical power are linked to the following:

a. Photodiode voltage drop and swing: Part of the applied bias voltage is lost because of the voltage drop in the series resistance and voltage swing in the load resistance.
b. Space charge effect: Under high current injection, the electric field is reduced at the collector input.
c. Thermal limitation: Photodiode temperature increases at high optical power due to heat dissipation.

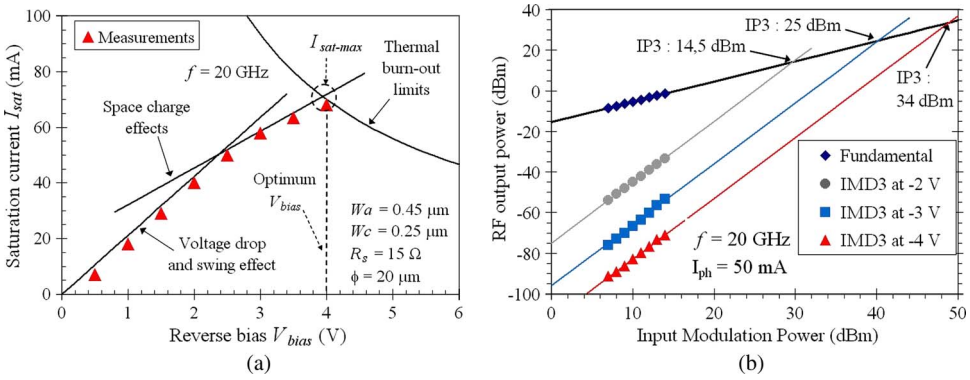

Fig. 6. (a) 1-dB saturation photocurrent at 20 GHz versus Vbias of a power UTC and (b) comparison of IMD3 measurements for various reverse bias at Iph = 50 mA.

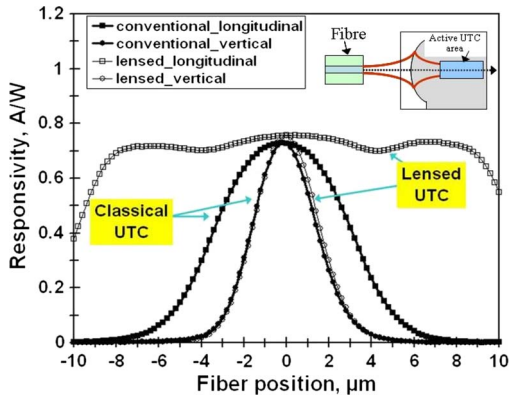

Fig. 7. Responsivity comparison of a 5×25 μm^2 classical photodiode with lensed photodiode.

Fig. 6(a) displays the 1-dB saturation currents at 20 GHz versus reverse bias of a typical high power UTC photodiode. We also show the thermal burn-out limits, the voltage drop, and swing limitations (Vop = 0 V), as well as the space charge limitations represented by the lower limit of the electric field (a 10 kV/cm: higher field is necessary for carriers to drift at saturation velocity). From this model, we can predict the saturation photocurrent from the intersecting between thermal limits and space charge effect limitations.

Coming now to linear operation, a specific two-tone setup is necessary to assess analog operation of UTC photodiodes by measuring third-order intermodulation distortion IMD3 [15]. Fig. 6(b) shows typical IMD3 measurement results at a large photocurrent of 50 mA and for various reverse biases. As a convention, the third-order intercept point (IP3) is extrapolated from the fundamental signal (line of slope 1) and the third-order intermodulation distortion IMD3 signal (line of slope 3). The diode linearity assessed through IP3 (third-order intercept point) is extrapolated from the IMD3 signal and the fundamental signal and shows a large 34-dBm IP3 at 20 GHz and 4-V reverse bias. As for saturation measurements, the linearity of the high-power detectors is improved by increasing applied reverse bias.

For applications requiring > 40-GHz bandwidth, lateral illumination is preferred using a waveguide structure. A specific monolithic integrated lens achieved by dry etching of the mirror facet allows increasing coupling efficiency and tolerances with an optical fiber, as demonstrated through comparison of fiber tolerances of a conventional straight mirror facet and a lensed mirror facet. Fig. 7 presents the responsivity-tolerance measurements (at a wavelength of 1.55 μm) for both 5×25 μm^2 conventional and lensed photodiodes with a waveguide length > 25 μm tested with a 5-μm-mode-diameter lensed fiber. As clearly shown in Fig. 7, a significant difference in the lateral

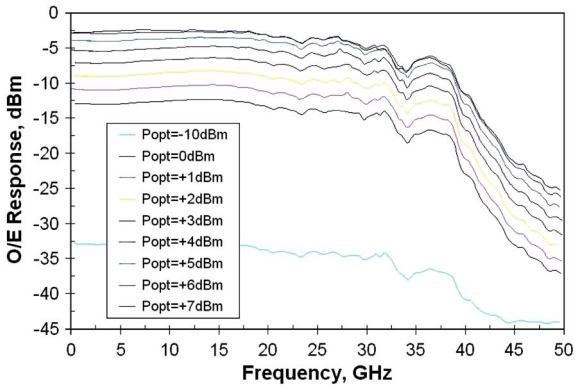

Fig. 8. O/E response of the lensed dual-UTC linear photoreceiver.

profiles is found between the two structures. The 1-dB fiber alignment tolerance is > 20 μm in the lateral direction for the lensed structure, whereas the tolerance is 5 μm for the conventional structure. This significant improvement of coupling tolerances allows reducing the imbalance between two adjacent photodiodes in dual-photoreceiver configuration. In addition, pigtailing of such dual photodiodes involves an adjusted path-length fiber ribbon positioned in silicon V-grooves. The monolithic lens avoids the rotating fiber ribbon to improve coupling efficiency and contributes, therefore, to reducing the overall cost of the module assembly. The responsivity of the lensed UTC photodiode is as high as 0.76 A/W (polarization dependence below 0.3 dB), which is larger than the conventional photodiode (0.71 A/W) due to reduced lateral divergence.

Fig. 8 shows the frequency response of the balanced UTC linear photoreceiver for optical input powers ranging from -10 dBm to $+7$ dBm. The 3-dB bandwidth is > 30 GHz for all investigated optical input powers. This linear operation is very useful for further digital signal processing (signal distortion compensation, ...).

4. Conclusion

The rapid development in communication technologies, including fiber optic networks, analog microwave links, or new applications like ranging and sensors, is driving an increased demand for InGaAs photodiodes. This key absorption material is used today in various vertical designs of detectors: For high-sensitivity photoreceivers, avalanche multiplication in large-bandgap AlInAs material with an InGaAs absorber demonstrates record gain–bandwidth product and low excess noise. The InGaAs/InP UTC diode provides the best-in-class power operation at microwave frequencies.

References

[1] T. Pearsall, "Photodetectors for communication by optical fibres," in *Optical Fibre Communications*, M. J. Howes and D. V. Morgan, Eds. New York: Wiley, 1980.
[2] J. E. Bowers and C. A. Burrus, "Ultrawide-band long-wavelength p-i-n photodetectors," *J. Lightwave Technol.*, vol. 5, no. 10, pp. 1339–1350, Oct. 1987.
[3] R. J. McIntyre, "Multiplication noise in uniform avalanche diodes," *IEEE Trans. Electron Devices*, vol. ED-13, no. 1, pp. 164–168, Jan. 1966.
[4] M. A. Itzler, K. K. Loi, S. McCoy, N. Codd, and N. Komaba, "High-performance, manufacturable avalanche photodiodes for 10 Gb/s optical receivers," in *Proc. 25th OFC*, 2000, vol. 4, pp. 126–128, Paper FG5.
[5] B. K. Ng, J. P. R. David, R. C. Tozer, M. Hopkinson, G. Hill, and G. J. Rees, "Excess noise characteristics of $Al_{0.8}Ga_{0.2}As$ avalanche photodiodes," *IEEE Photon. Technol. Lett.*, vol. 14, no. 4, pp. 522–524, Apr. 2002.
[6] Y. L. Goh, A. R. J. Marshall, D. J. Massey, J. S. Ng, C. H. Tan, M. Hopkinson, J. P. R. David, S. K. Jones, C. C. Button, and S. M. Pinches, "Excess avalanche noise in $In_{0.52}Al_{0.48}As$," *IEEE J. Quantum Electron.*, vol. 43, no. 6, pp. 503–507, Jun. 2007.
[7] K. J. Williams and D. Esman, "Large-signal compression-current measurements in high-power microwave pin photodiodes," *Electron. Lett.*, vol. 35, no. 1, pp. 82–84, Jan. 1999.

[8] X. Li, N. Li, S. Demiguel, J. C. Campbell, D. Tulchinsky, and K. J. Williams, "A comparison of front- and backside-illuminated high-saturation power partially depleted absorber photodetectors," *IEEE J. Quantum Electron.*, vol. 40, no. 9, pp. 1321–1325, Sep. 2004.
[9] H. Ito, S. Kodama, Y. Muramoto, T. Furuta, T. Nagatsuma, and T. Ishibashi, "High-speed and high-output InP-InGaAs unitraveling-carrier photodiodes," *IEEE J. Sel. Topics Quantum Electron.*, vol. 10, no. 4, pp. 709–727, Jul./Aug. 2004.
[10] M. Chtioui, A. Enard, D. Carpentier, S. Bernard, B. Rousseau, F. Lelarge, F. Pommereau, and M. Achouche, "High-power high-linearity uni-traveling-carrier photodiodes for analog photonic links," *IEEE Photon. Technol. Lett.*, vol. 20, no. 3, pp. 202–204, Feb. 2008.
[11] E. Yagyu, E. Ishimura, M. Nakaji, T. Aoyagi, and Y. Tokuda, "Simple planar structure for high-performance AlInAs avalanche photodiodes," *IEEE Photon. Technol. Lett.*, vol. 18, no. 1, pp. 76–78, Jan. 2006.
[12] A. Rouvié, D. Carpentier, J. Décobert, N. Lagay, P. Pommereau, and M. Achouche, "Low noise and high gain-bandwidth product AlInAs avalanche photodiodes," in *Proc. 20th IPRM*, 2008, pp. 1–4.
[13] H. Ito, H. Fushimi, Y. Muramoto, T. Furuta, and T. Ishibashi, "High-power photonic microwave generation at K- and Ka-bands using a uni-traveling-carrier photodiodes," *J. Lightwave Technol.*, vol. 20, no. 8, pp. 1500–1505, Aug. 2002.
[14] N. Duan, X. Wang, N. Li, H. D. Liu, and J. C. Campbell, "Thermal analysis of high-power InGaAs–InP photodiodes," *IEEE J. Quantum Electron.*, vol. 42, no. 12, pp. 1255–1258, Dec. 2006.
[15] M. Chtioui, A. Enard, D. Carpentier, S. Bernard, B. Rousseau, F. Lelarge, F. Pommereau, and M. Achouche, "High-performance uni-traveling-carrier photodiodes with a new collector design," *IEEE Photon. Technol. Lett.*, vol. 20, no. 13, pp. 1163–1165, Jul. 2008.